AD-A157 248 AN EVALUATION OF FOUR METHODS OF NUMERICAL ANALYSIS FOR TWO-DIMENSIONAL A.. (U) DAVID W TAYLOR NAVAL SHIP RESEARCH AND DEVELOPMENT CENTER BET.. R BURKE 1/1

UNCLASSIFIED 06 JUL 85 DTNSRDC/SPD-1139-01-REV F/G 9/2 NL

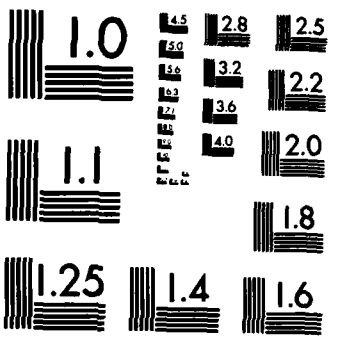

(2)

DAVID W. TAYLOR NAVAL SHIP RESEARCH AND DEVELOPMENT CENTER

Bethesda, Maryland 20084

AD-A157 248

AN EVALUATION OF FOUR METHODS OF NUMERICAL ANALYSIS FOR TWO-DIMENSIONAL AIRFOIL FLOWS

Roger Burke

APPROVED FOR PUBLIC RELEASE: DISTRIBUTION UNLIMITED
DAVID TAYLOR NAVAL SHIP R & D CENTER (CODE 15)

SHIP PERFORMANCE DEPARTMENT

DEPARTMENTAL REPORT

July 1985

SPD-1139-01
Revised Jul6 1985

MAJOR DTNSRDC ORGANIZATIONAL COMPONENTS

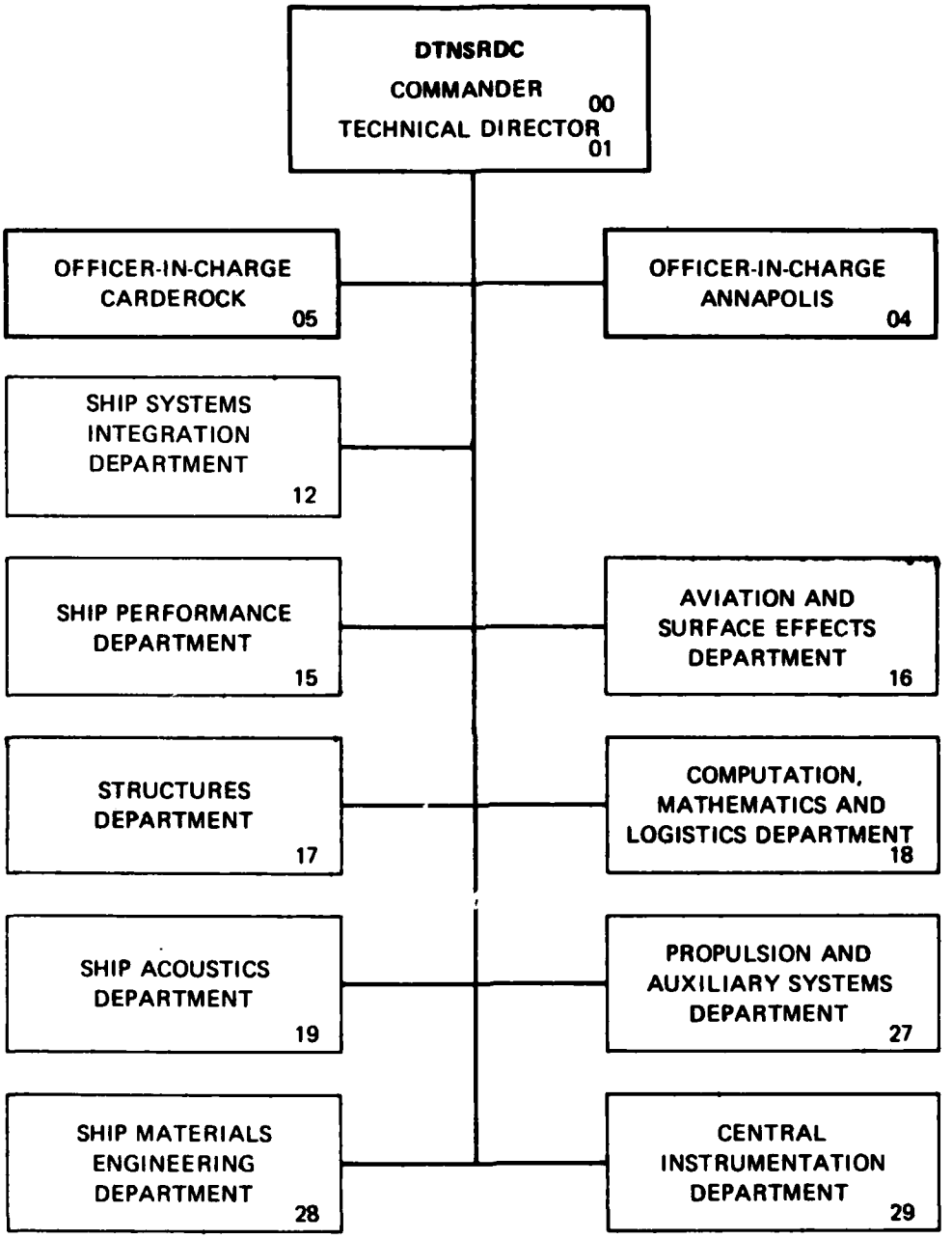

GPO 866 987

NDW-DTNSRDC 5602/21 (2-80)

REPORT DOCUMENTATION PAGE

1a. REPORT SECURITY CLASSIFICATION Unclassified	1b. RESTRICTIVE MARKINGS
2a. SECURITY CLASSIFICATION AUTHORITY	3 DISTRIBUTION / AVAILABILITY OF REPORT Approved for Public Release: Distribution Unlimited
2b. DECLASSIFICATION / DOWNGRADING SCHEDULE	
4 PERFORMING ORGANIZATION REPORT NUMBER(S) SPD-1139-01	5. MONITORING ORGANIZATION REPORT NUMBER(S)
6a. NAME OF PERFORMING ORGANIZATION David W. Taylor Naval Ship R & D Center 6b. OFFICE SYMBOL (If applicable)	7a. NAME OF MONITORING ORGANIZATION (Code 56XN3) Naval Sea Systems Command
6c. ADDRESS (City, State, and ZIP Code) Bethesda, MD 20084	7b. ADDRESS (City, State, and ZIP Code) Washington D.C. 20362
8a. NAME OF FUNDING / SPONSORING ORGANIZATION Code 56XN3 Naval Sea Systems Command 8b. OFFICE SYMBOL (If applicable)	9. PROCUREMENT INSTRUMENT IDENTIFICATION NUMBER
8c. ADDRESS (City, State, and ZIP Code) Washington, D.C. 20362	10 SOURCE OF FUNDING NUMBERS PROGRAM ELEMENT NO. 62561N; PROJECT NO; TASK NO. S1266001; WORK UNIT ACCESSION NO 1544-382

11 TITLE (Include Security Classification)

An Evaluation of Four Methods of Numerical Analysis for Two-Dimensional Airfoil Flows

12 PERSONAL AUTHOR(S)
Roger Burke

13a TYPE OF REPORT	13b TIME COVERED	14. DATE OF REPORT (Year, Month, Day)	15. PAGE COUNT
Departmental Report	FROM _____ TO _____	July 1985	26

16 SUPPLEMENTARY NOTATION

17 COSATI CODES			18 SUBJECT TERMS (Continue on reverse if necessary and identify by block number)
FIELD	GROUP	SUB-GROUP	Airfoil analysis, computer code

19 ABSTRACT (Continue on reverse if necessary and identify by block number)

Four computer programs for analyzing the inviscid and boundary layer flow over two dimensional airfoils are exercised in comparisons against experimental data from two wind tunnel studies. The solution method of each computer program is discussed, followed by a description of the airfoil geometries used in the model comparisons. Measured values of pressure distribution, turbulent separation point, and boundary layer properties are compared against predicted values.

20 DISTRIBUTION / AVAILABILITY OF ABSTRACT ☒ UNCLASSIFIED/UNLIMITED ☐ SAME AS RPT ☐ DTIC USERS	21 ABSTRACT SECURITY CLASSIFICATION Unclassified
22a NAME OF RESPONSIBLE INDIVIDUAL Roger Burke	22b TELEPHONE (Include Area Code) (202) 227-1865 22c OFFICE SYMBOL

DD FORM 1473, 84 MAR 83 APR edition may be used until exhausted
All other editions are obsolete

ABSTRACT

Four computer programs for analyzing the inviscid and boundary layer flow over two dimensional airfoils are exercised in comparisons against experimental data from two wind tunnel studies. The solution method of each computer program is discussed, followed by a description of the airfoil geometries used in the model comparisons. Measured values of pressure distribution, turbulent separation point, and boundary layer properties are compared against predicted values.

ADMINISTRATIVE INFORMATION

The work presented in this report was conducted with funding from Naval Sea Systems Command (56xN) under Task Area S1266001, Program Element 63561N, and Work Unit 1544-382-75 at the David W. Taylor Naval Ship Research and Development Center (DTNSRDC).

INTRODUCTION

This report compares four computer codes for predicting the flow over two dimensional airfoils. One of the codes obtains the inviscid flow using panel methods, and the boundary layer flow using integral methods. It is the only code considered here that includes both inviscid and boundary layer routines. Another code computes the inviscid flow, also using panel methods, but does not have a boundary layer routine. The remaining two codes calculate the vertical variation of flow variables within the boundary layer using finite differences; the external inviscid flow is not computed, and must be included in the program input.

After a brief discussion of the solution method of each computer code, numerical predictions are compared against experimental data from two wind tunnel studies, involving four airfoil geometries, each of which experiences trailing edge separation. The airfoil shapes are described, and comparisons made between measured and predicted values of pressure, turbulent separation, and boundary layer parameters.

COMPUTER CODES

The computer codes used in the comparisons are designated as follows: (1) Chang potential flow, by M.S. Chang and Y.T. Shen (reference 1); (2) Eppler potential and integral code, by R. Eppler and D.M. Somers (reference 2); Cebeci eddy viscosity code, by T. Cebeci (reference 3), and (4) Cebeci κ-ε code, by T. Cebeci (reference 4).

A brief description of each of the codes will be given below; detailed explanations may be found in the references cited above. The Chang potential flow code divides the foil surface into panels, each of which is represented by a vortex distribution and two source distributions. The pressures and the forces on the foil are then computed from the resulting induced potential field through use of Bernoullis equation. The Eppler potential code calculates the potential flow field using a method of vorticity distributed over a foil surface. The inviscid flow solution then serves as input to an integral method analysis of the boundary layer. The Cebeci eddy and κ-ε codes embody a finite difference representation of the boundary layer equations, with turbulence closure being achieved through either an eddy viscosity formulation or a two equation κ-ε approach, where κ is the turbulent kinetic energy, and ε the turbulent dissipation. Unlike the Eppler integral code, the eddy viscosity and κ-ε codes do not calculate the potential flow field around the airfoil, which must be supplied as part of the input.

A summary of the solution approach and boundary layer scheme for each of the computer codes is given in Table 1. As seen from this table, none of the codes considered here includes an iterative approach tor handling boundary layer displacement effects. An iterative approach generally involves a process of: (1) calculating the inviscid flow solution around the original airfoil surface, (2) calculating the boundary layer solution based on the inviscid solution, (3) recalculating the inviscid flow solution with a modified airfoil shape, obtained by adding the boundary layer displacement thickness to the airfoil, and (4) repeating steps 2 and 3 until convergence criteria are satisified.

Various input parameters are required by the computer codes in order to simulate the experimental flow conditions experienced in the wind tunnel studies.

COMPUTER CODE	SOLUTION APPROACH	BOUNDARY LAYER CHARACTERISTICS			
		Laminar	Transisition	Turbulence	Viscid/Inviscid Interaction
Chang potential	Distributed vorticity over airfoil shape	N/A	N/A	N/A	N/A
Cebeci eddy viscosity	Two dimensional boundary layer equations approximated using finite differences, and solved using two-point Box Method (Cebeci et al., 1977)	YES	natural or fixed	eddy viscosity	NO
Cebeci κ-ε	Same as eddy viscosity code	NO	NO	κ-ε	NO
Eppler potential and integral	Distributed vorticity over airfoil shape approximated by curved panels.	YES	natural or fixed	Empirical	NO

TABLE 1 - Comparison of Four Airfoil Codes

A zero angle of attack was assumed for use in the Chang and Eppler potential flow codes. The experimental Cp distribution served as input to the eddy viscosity and κ-ε codes, which require specification of the pressure distribution over the foil surface. The airfoil surfaces were assumed hydraulically smooth. The natural transition mode was used in the eddy viscosity and Eppler integral codes to determine the location of transition from laminar to turbulent flow; in the κ-ε code, which does not compute transition, the calculations were started at a chord location where the flow was turbulent, as determined from the eddy viscosity code results. The free stream velocity, Uo, was specified in accordance with that recorded in the wind tunnel studies.

AIRFOIL SECTIONS

Four airfoil geometries are considered in the model comparisons. Three of the airfoils correspond to geometries analyzed by Blake (1975) in a wind tunnel study of flow over interchangeable trailing edge sections, which were attached to a working strut 3 feet in length and 4 feet in span, with a circular leading edge 2 inches in diameter. The strut and trailing edge designs are shown in Figure 1, where the designs are denoted as T45, T25S and T25R. The T45 edge is four inches in length, has a 45° included tip angle, and a circular arc of 5 inch radius joining the tip and middle section. The T25R trailing edge has a similar design with a 25 degree included tip angle, a 6.25 inch length, and a 10-inch radius circle joining the parallel middle to the tip. The remaining tip, T25S, is composed of two additional inches of parallel middle body joining a segment 4.25 inches in length with a 25 degree included tip angle. The equations formulated to define the trailing edge shapes and their domain of definition are taken from Groves (unpublished, 1983), and given in Table 2. The x and y coordinates are in the dimensions of inches, with the origin at the midpoint of the circular leading edge. The discrete set of cordinates, nondimensionalized by the chord length, are given in Tables 3, 4, and 5. In this reference frame the nose has the ordinates x = o, y = o, and the trailing edge tip point has the ordinate x = 1. The order in which the offsets are given is leading edge, upper surface, lower surface, and leading edge.

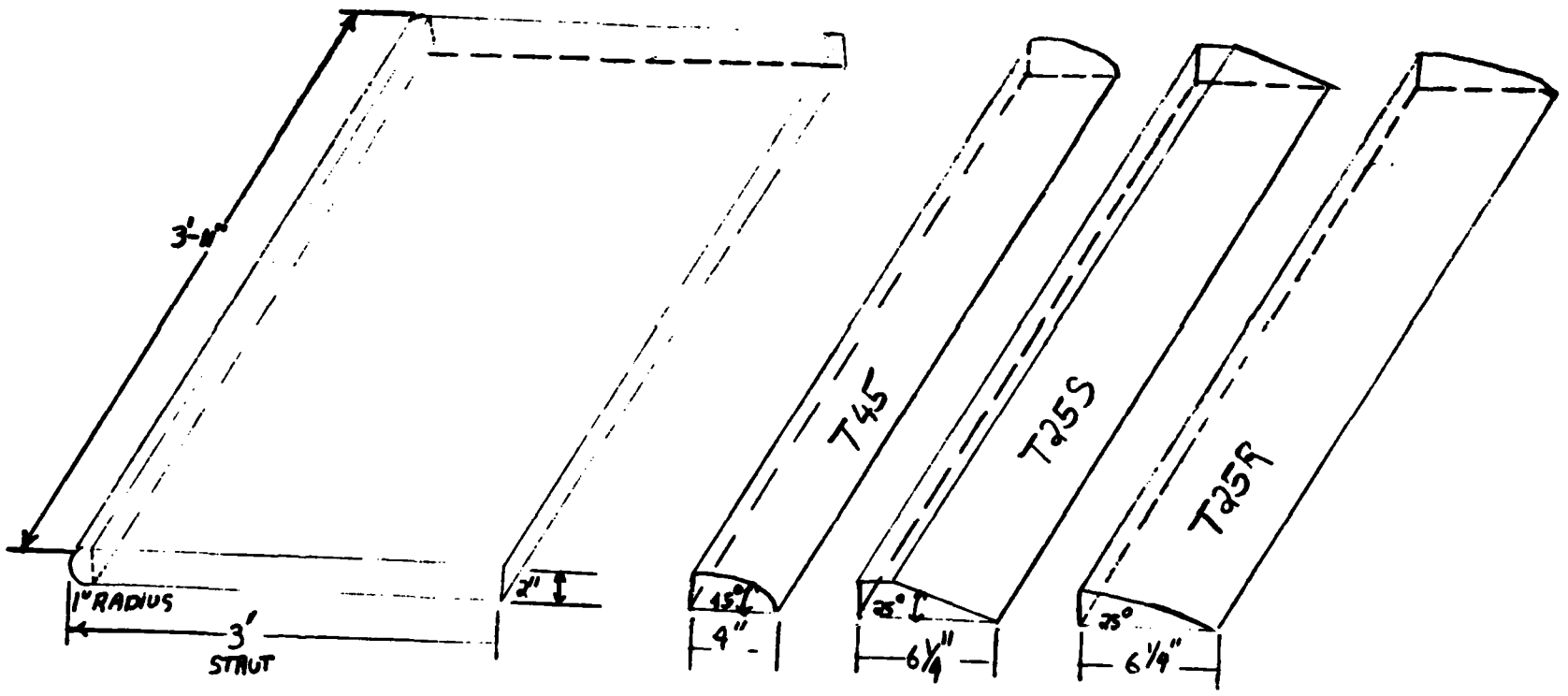

FIGURE 1 - A view of the working strut showing orientation of trailing edge sections.

Trailing Edge	DEFINING EQUATION (X and Y are in inches)	Domain of Definition (inches)
T45	$(X-36)^2 + (Y + 4)^2 = 25$	$36 \leq X \leq 39$
	$Y = (39 - X)$	$39 \leq X \leq 40$
T25S	$Y = 1.0$	$36 \leq X \leq 38$
	$Y = -0.46631(X-42.25)-1.0$	$38 \leq X \leq 42.25$
T25R	$(X - 36)^2 + (Y + 9)^2 = 100$	$36 \leq X \leq 38.85$
	$Y = -0.46631(X-42.25)-1.0$	$38.85 \leq X \leq 42.25$

TABLE 2 - Equations for Trailing Edge Offsets

TABLE 3 - T45 OFFSETS

UPPER SURFACE		LOWER SURFACE	
X	Y	X	Y
0.0000	0.0000	0.9973	-0.0250
0.0004	0.0043	0.9937	-0.0250
0.0015	0.0086	0.9887	-0.0250
0.0033	0.0125	0.9825	-0.0250
0.0058	0.0161	0.9750	-0.0250
0.0089	0.0192	0.9663	-0.0250
0.0125	0.0216	0.9575	-0.0250
0.0165	0.0235	0.9488	-0.0250
0.0207	0.0246	0.9400	-0.0250
0.0250	0.0250	0.9300	-0.0250
0.0300	0.0250	0.9200	-0.0250
0.0375	0.0250	0.9100	-0.0250
0.0562	0.0250	0.9000	-0.0250
0.0844	0.0250	0.8825	-0.0250
0.1265	0.0250	0.8625	-0.0250
0.1900	0.0250	0.8350	-0.0250
0.2850	0.0250	0.8000	-0.0250
0.3800	0.0250	0.7550	-0.0250
0.4750	0.0250	0.7000	-0.0250
0.5600	0.0250	0.6350	-0.0250
0.6350	0.0250	0.5600	-0.0250
0.7000	0.0250	0.4750	-0.0250
0.7550	0.0250	0.3800	-0.0250
0.8000	0.0250	0.2850	-0.0250
0.8350	0.0250	0.1900	-0.0250
0.8625	0.0250	0.1265	-0.0250
0.8825	0.0250	0.0844	-0.0250
0.9000	0.0250	0.0562	-0.0250
0.9100	0.0246	0.0375	-0.0250
0.9200	0.0234	0.0300	-0.0250
0.9300	0.0214	0.0250	-0.0250
0.9400	0.0184	0.0207	-0.0246
0.9488	0.0151	0.0165	-0.0235
0.9575	0.0110	0.0125	-0.0216
0.9663	0.0060	0.0089	-0.0192
0.9750	0.0000	0.0058	-0.0161
0.9825	-0.0075	0.0033	-0.0125
0.9887	-0.0137	0.0015	-0.0086
0.9937	-0.0188	0.0004	-0.0043
0.9973	-0.0223	0.0000	0.0000
1.0000	-0.0250		

UPPER SURFACE		LOWER SURFACE	
X	Y	X	Y
0.0000	0.0000	0.9981	-0.0237
0.0004	0.0041	0.9960	-0.0237
0.0014	0.0081	0.9934	-0.0237
0.0032	0.0118	0.9901	-0.0237
0.0055	0.0152	0.9863	-0.0237
0.0085	0.0181	0.9818	-0.0237
0.0118	0.0205	0.9771	-0.0237
0.0156	0.0222	0.9721	-0.0237
0.0196	0.0233	0.9669	-0.0237
0.0237	0.0237	0.9614	-0.0237
0.0284	0.0237	0.9550	-0.0237
0.0355	0.0237	0.9479	-0.0237
0.0532	0.0237	0.9408	-0.0237
0.0799	0.0237	0.9326	-0.0237
0.1198	0.0237	0.9262	-0.0237
0.1799	0.0237	0.9191	-0.0237
0.2698	0.0237	0.9131	-0.0237
0.3598	0.0237	0.9084	-0.0237
0.4497	0.0237	0.9044	-0.0237
0.5302	0.0237	0.9013	-0.0237
0.6012	0.0237	0.8982	-0.0237
0.6627	0.0237	0.8952	-0.0237
0.7148	0.0237	0.8911	-0.0237
0.7574	0.0237	0.8864	-0.0237
0.7905	0.0237	0.8805	-0.0237
0.8639	0.0237	0.8355	-0.0237
0.8734	0.0237	0.8166	-0.0237
0.8805	0.0237	0.7905	-0.0237
0.8864	0.0237	0.7574	-0.0237
0.8911	0.0237	0.7148	-0.0237
0.8952	0.0237	0.6627	-0.0237
0.8982	0.0237	0.6012	-0.0237
0.9013	0.0224	0.5302	-0.0237
0.9044	0.0209	0.4497	-0.0237
0.9084	0.0190	0.3598	-0.0237
0.9131	0.0168	0.2698	-0.0237
0.9191	0.0141	0.1799	-0.0237
0.9262	0.0108	0.1198	-0.0237
0.9326	0.0078	0.0799	-0.0237
0.9408	0.0039	0.0532	-0.0237
0.9479	0.0006	0.0355	-0.0237
0.9550	-0.0027	0.0284	-0.0237
0.9614	-0.0057	0.0237	-0.0237
0.9669	-0.0083	0.0196	-0.0233
0.9721	-0.0106	0.0156	-0.0222
0.9771	-0.0129	0.0118	-0.0205
0.9818	-0.0151	0.0085	-0.0181
0.9863	-0.0172	0.0055	-0.0152
0.9901	-0.0190	0.0032	-0.0118
0.9934	-0.0206	0.0014	-0.0081
0.9960	-0.0218	0.0004	-0.0041
0.9981	-0.0228	0.0000	0.0000
1.0000	-0.0237		

TABLE 5 - T2SR OFFSETS

UPPER SURFACE		LOWER SURFACE	
X	Y	X	Y
0.0000	0.0000	0.9974	-0.0237
0.0004	0.0041	0.9936	-0.0237
0.0014	0.0081	0.9891	-0.0237
0.0032	0.0118	0.9837	-0.0237
0.0055	0.0152	0.9780	-0.0237
0.0085	0.0181	0.9721	-0.0237
0.0118	0.0205	0.9659	-0.0237
0.0156	0.0222	0.9595	-0.0237
0.0196	0.0233	0.9529	-0.0237
0.0237	0.0237	0.9463	-0.0237
0.0284	0.0237	0.9394	-0.0237
0.0355	0.0237	0.9323	-0.0237
0.0532	0.0237	0.9250	-0.0237
0.0799	0.0237	0.9174	-0.0237
0.1198	0.0237	0.9096	-0.0237
0.1799	0.0237	0.9015	-0.0237
0.2698	0.0237	0.8930	-0.0237
0.3598	0.0237	0.8840	-0.0237
0.4497	0.0237	0.8746	-0.0237
0.5302	0.0237	0.8629	-0.0237
0.6012	0.0237	0.8521	-0.0237
0.6627	0.0237	0.8355	-0.0237
0.7148	0.0237	0.8166	-0.0237
0.7574	0.0237	0.7905	-0.0237
0.7905	0.0237	0.7574	-0.0237
0.8166	0.0237	0.7148	-0.0237
0.8355	0.0237	0.6627	-0.0237
0.8521	0.0237	0.6012	-0.0237
0.8629	0.0234	0.5302	-0.0237
0.8746	0.0226	0.4497	-0.0237
0.8840	0.0215	0.3598	-0.0237
0.8930	0.0201	0.2698	-0.0237
0.9015	0.0184	0.1799	-0.0237
0.9096	0.0166	0.1198	-0.0237
0.9174	0.0145	0.0799	-0.0237
0.9250	0.0119	0.0532	-0.0237
0.9323	0.0079	0.0355	-0.0237
0.9394	0.0046	0.0284	-0.0237
0.9463	0.0014	0.0237	-0.0237
0.9529	-0.0017	0.0196	-0.0233
0.9595	-0.0048	0.0156	-0.0222
0.9659	-0.0078	0.0118	-0.0205
0.9721	-0.0106	0.0085	-0.0181
0.9780	-0.0131	0.0055	-0.0152
0.9837	-0.0152	0.0032	-0.0118
0.9891	-0.0169	0.0014	-0.0081
0.9936	-0.0182	0.0004	-0.0041
0.9974	-0.0191	0.0000	0.0000
1.0000	-0.0197		

The fourth airfoil geometry used in the comparisons is a modified NACA 0012, designated as AB5. The trailing edge shape is shown in Figure 2, and the ordinates are given in Table 6.

Although no attempt has been made here to investigate the sensitivity of the computational results of the computer codes with respect to airfoil offset density, it is believed that a sufficient number of points were used to obtain consistent, reliable results. A greater density of ordinates was placed in those regions having the greatest airfoil curvature, where the flow quantities would be expected to change most rapidly.

PRESSURE DISTRIBUTION

The pressure coefficient (C_p) distribution as determined by the Eppler and Chang potential codes for the four airfoil geometries is shown in Figures 3-6. Here,

$$C_p = (P-Po)/.5\rho Uo^2$$

where P is the local static pressure, Po is the ambient pressure, ρ is the fluid density, and Uo the free stream reference velocity. The agreement between the pressure coefficients predicted by the two codes is seen from Figures 3-6 to be generally quite good. Also shown in Figures 3-5 are the experimental Cp distributions as determined by Blake (1975) for the upper airfoil surface.

As might be expected, the predicted pressure distributions for the T45, T25R, and T25S airfoils are fairly similar on the working strut forward of the trailing edge sections. A sharp static pressure minimum is predicted on the leading edge circular radius, followed by a steep adverse pressure gradient. Further downstream, the static pressure gradient varies slightly, becomes somewhat favorable forward of the trailing edge.

The magnitude of the pressure gradient on the trailing edge sections depends on edge shape. Figures 7-9 show expanded views of the predicted Cp distribution on the upper surface of the T45, T25R and T25S trailing sections, together with the experimental values. The numerical values exhibit a favorable pressure gradient upstream of the leading edge of the trailing section, followed by an adverse pressure gradient further downstream. This trend is most noticeable for T25S, where both codes predict a sharp pressure minimum at the knuckle (X = .9).

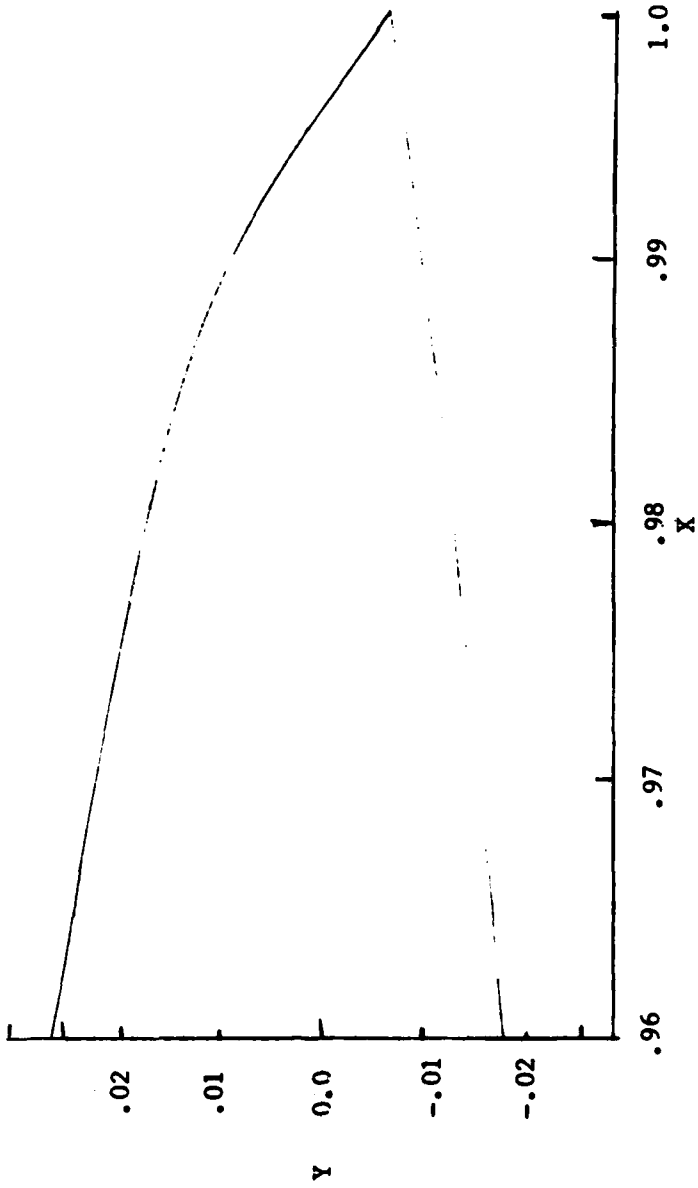

FIGURE 2 Trailing edge shape for AB5

TABLE 6 - ABS OFFSETS

UPPER SURFACE		LOWER SURFACE	
X	Y	X	Y
0.0000	0.0000	0.9925	-0.0071
0.0094	0.0091	0.9848	-0.0085
0.0250	0.0151	0.9812	-0.0090
0.0500	0.0215	0.9775	-0.0093
0.0750	0.0265	0.9737	-0.0097
0.1000	0.0305	0.9696	-0.0099
0.1500	0.0372	0.9667	-0.0105
0.2138	0.0436	0.9633	-0.0109
0.3000	0.0497	0.9600	-0.0113
0.3999	0.0541	0.9567	-0.0118
0.4999	0.0557	0.9533	-0.0119
0.5999	0.0543	0.9497	-0.0122
0.6799	0.0510	0.9469	-0.0125
0.7438	0.0464	0.9438	-0.0126
0.7999	0.0407	0.9406	-0.0130
0.8408	0.0352	0.9375	-0.0132
0.8736	0.0302	0.9333	-0.0138
0.8999	0.0260	0.9292	-0.0142
0.9125	0.0242	0.9250	-0.0145
0.9187	0.0230	0.9187	-0.0147
0.9250	0.0219	0.9125	-0.0154
0.9292	0.0208	0.8999	-0.0175
0.9333	0.0201	0.8736	-0.0199
0.9375	0.0195	0.8408	-0.0220
0.9406	0.0187	0.7999	-0.0241
0.9438	0.0178	0.7438	-0.0269
0.9469	0.0173	0.6799	-0.0293
0.9497	0.0169	0.5999	-0.0311
0.9533	0.0156	0.4999	-0.0319
0.9567	0.0149	0.3999	-0.0313
0.9600	0.0137	0.3000	-0.0293
0.9633	0.0125	0.2136	-0.0263
0.9667	0.0114	0.1500	-0.0232
0.9696	0.0101	0.1000	-0.0199
0.9737	0.0087	0.0750	-0.0178
0.9775	0.0066	0.0500	-0.0151
0.9812	0.0049	0.0250	-0.0113
0.9848	0.0032	0.0094	-0.0073
0.9925	-0.0011	0.0000	0.0000
1.0000	-0.0066		

Figure 3

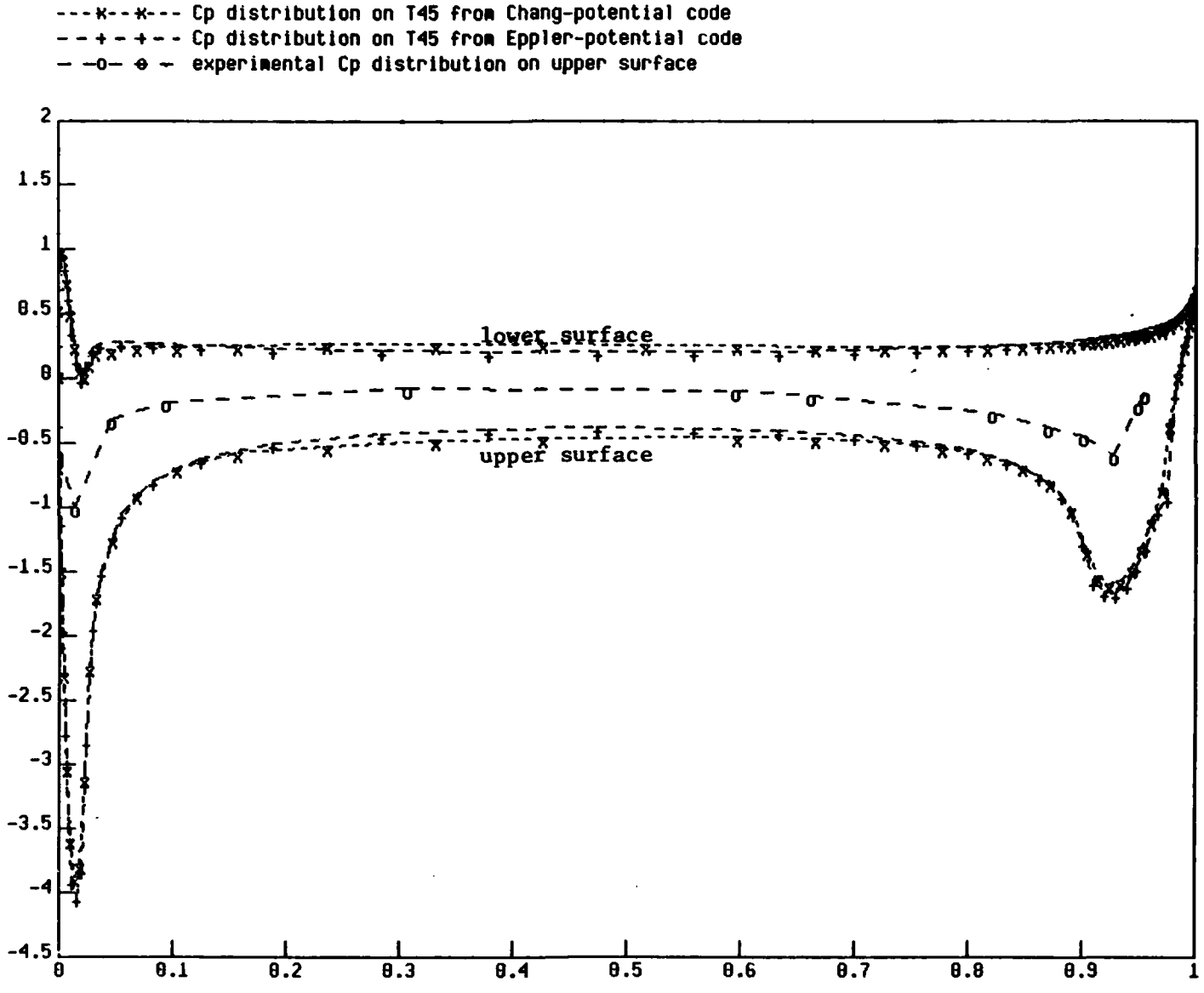
---x--x--- Cp distribution on T45 from Chang-potential code
- - + - + - - Cp distribution on T45 from Eppler-potential code
- -o- o - experimental Cp distribution on upper surface
lower surface
upper surface
2
1.5
1
0.5
0
-0.5
-1
-1.5
-2
-2.5
-3
-3.5
-4
-4.5
0
0.1
0.2
0.3
0.4
0.5
0.6
0.7
0.8
0.9
1

Figure 4

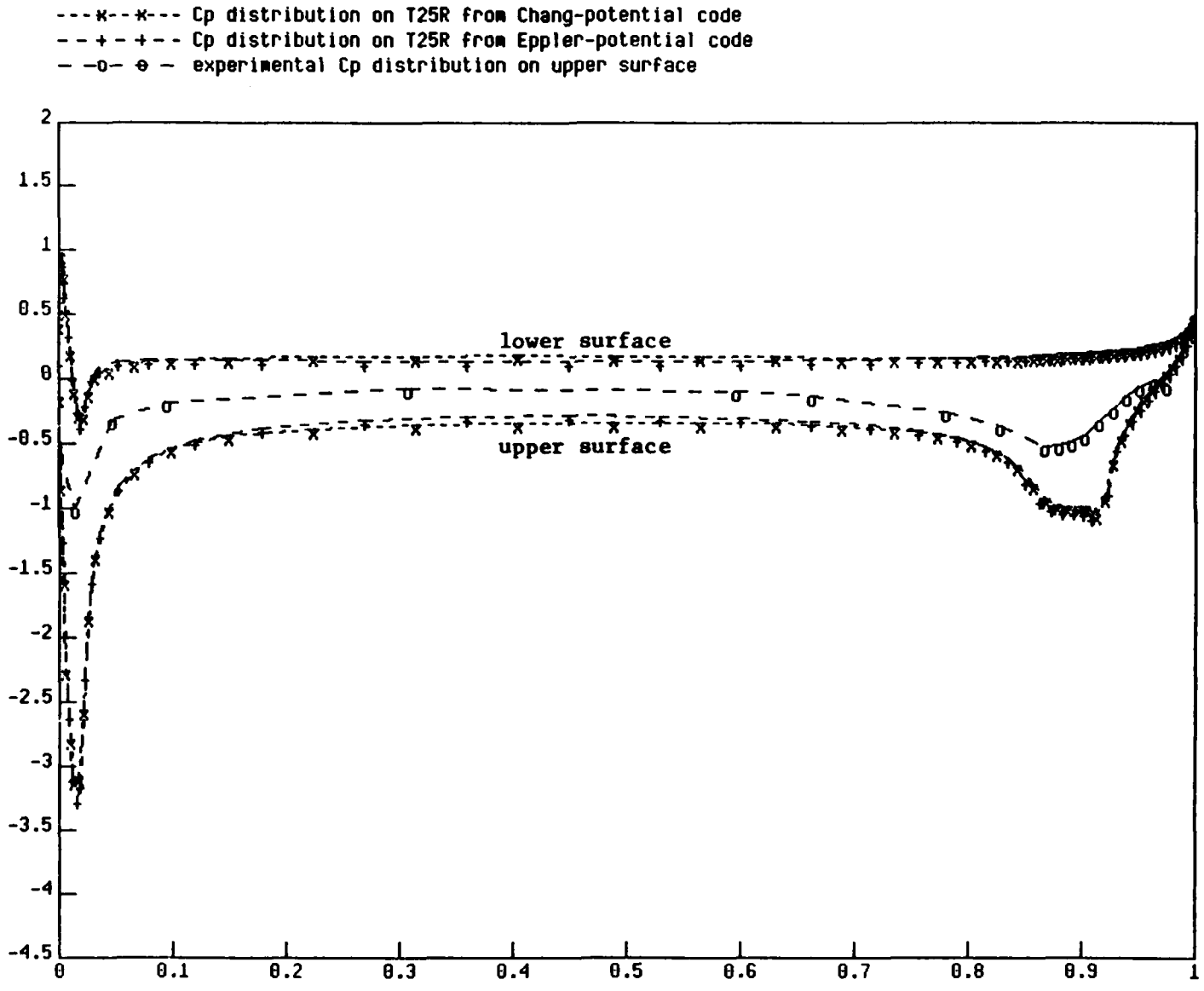
---x--x--- Cp distribution on T25R from Chang-potential code
- - + - + - - Cp distribution on T25R from Eppler-potential code
- -o- o - experimental Cp distribution on upper surface
lower surface
upper surface
2
1.5
1
0.5
0
-0.5
-1
-1.5
-2
-2.5
-3
-3.5
-4
-4.5
0
0.1
0.2
0.3
0.4
0.5
0.6
0.7
0.8
0.9
1

Figure 5

---x--x--- Cp distribution on T25S from Chang-potential code
- - + - + - - Cp distribution on T25S from Eppler-potential code
- -o- o -. experimental Cp distribution on upper surface

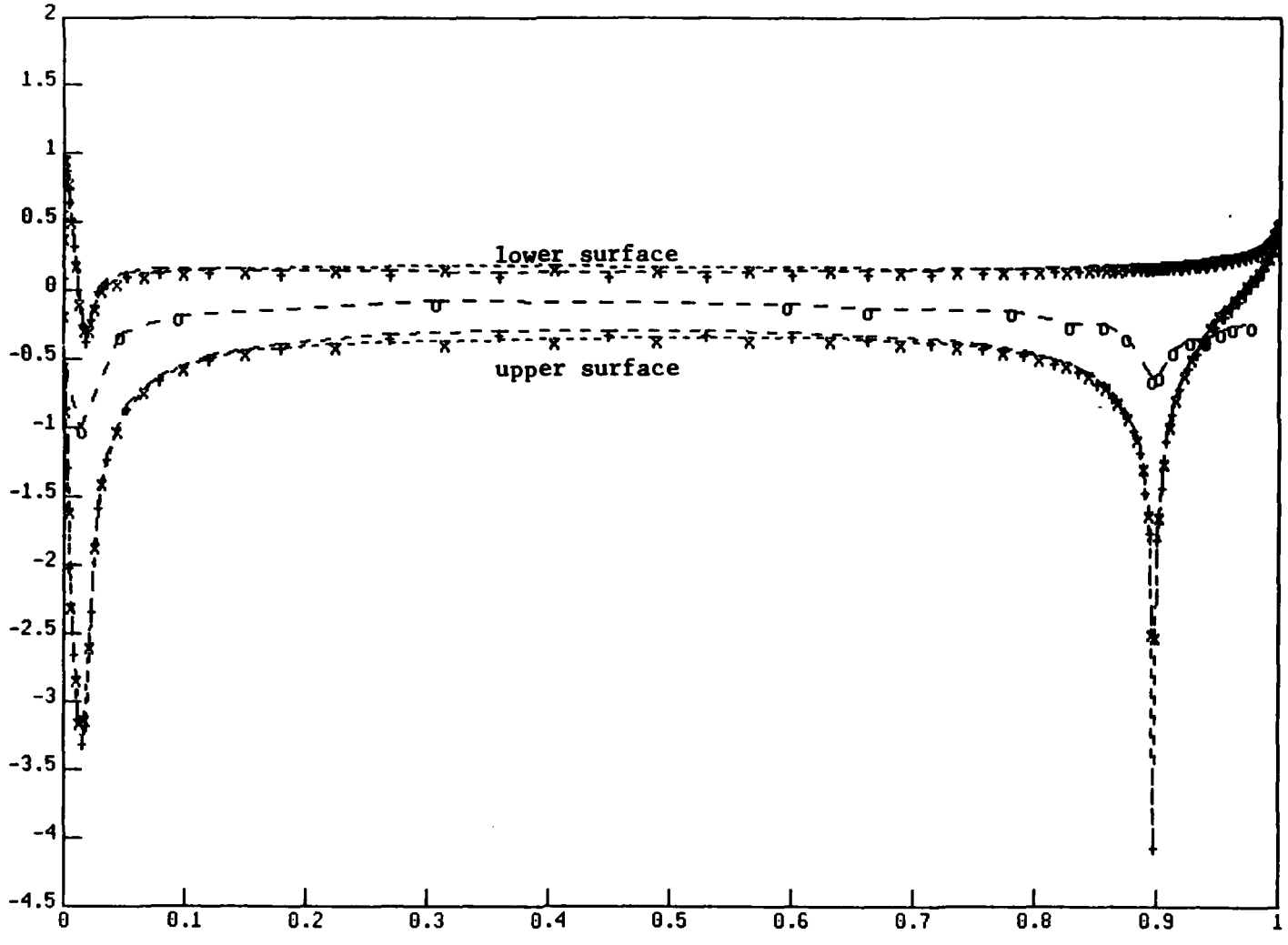

FIGURE 6 ---*--*--- Cp distribution on AB5 from Chang code
- - + - + - - Cp distribution on AB5 from Eppler code

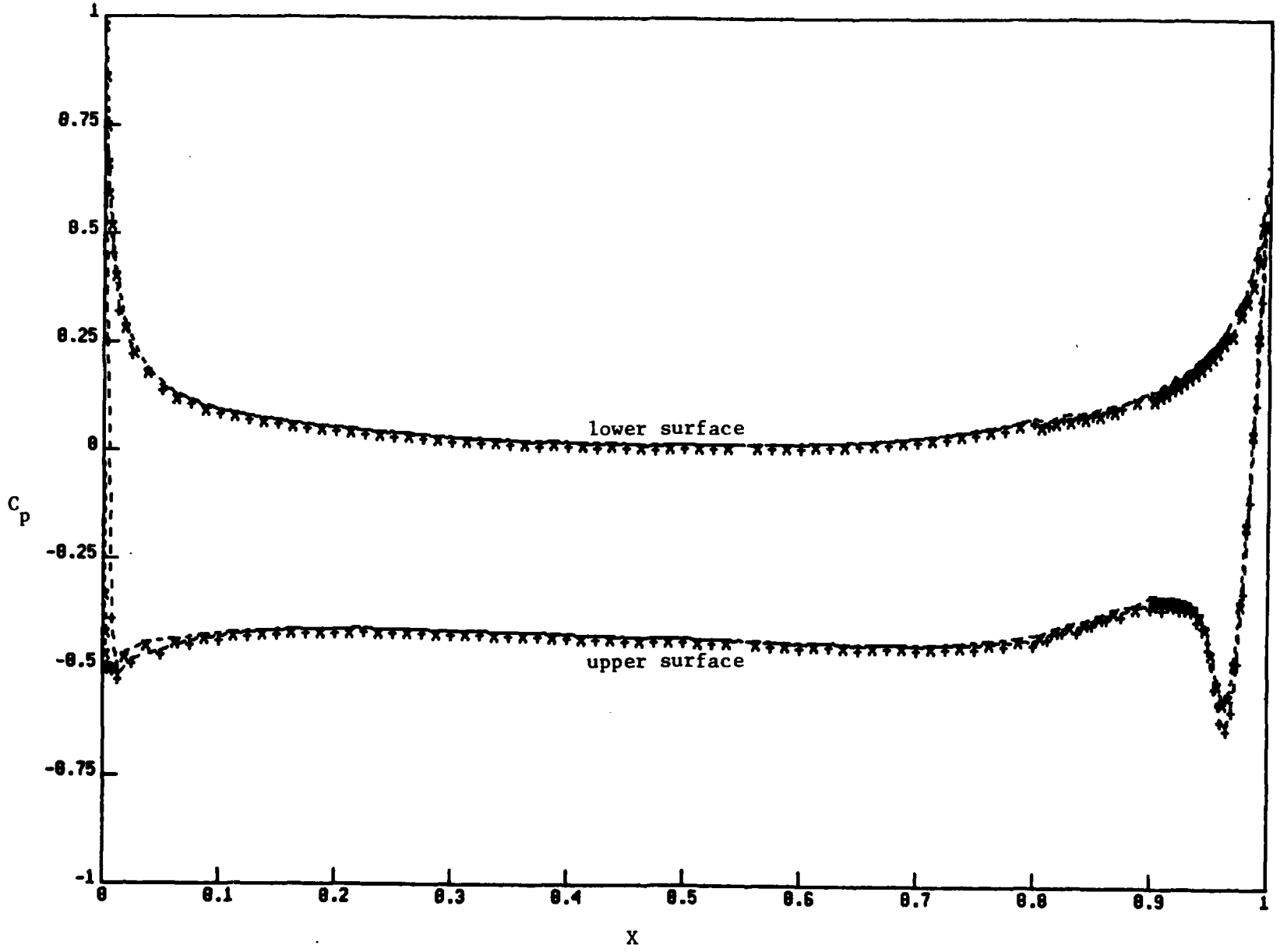

FIGURE 7

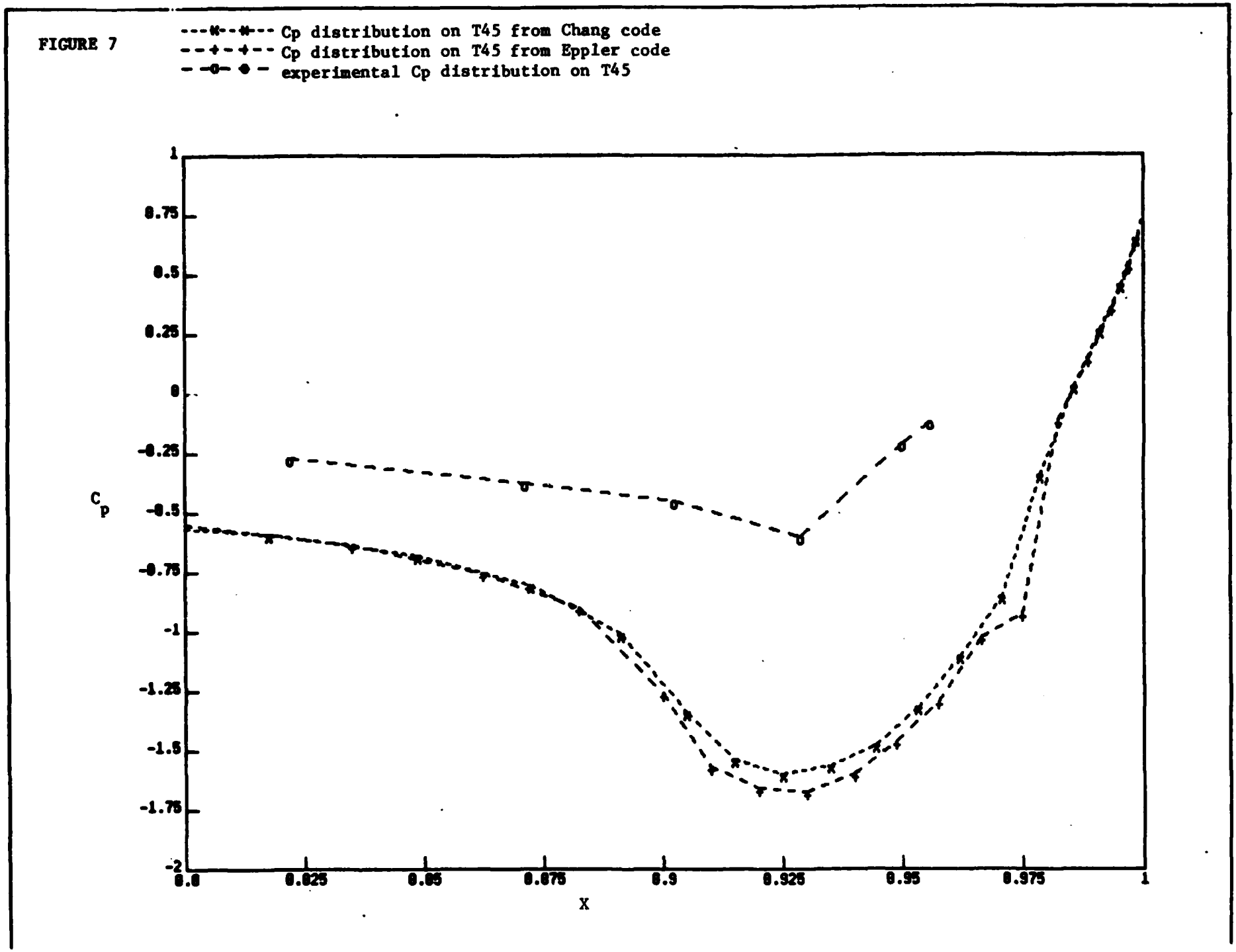
---*---*--- Cp distribution on T45 from Chang code
--+--+-- Cp distribution on T45 from Eppler code
--o--●-- experimental Cp distribution on T45
1
0.75
0.5
0.25
0
-0.25
-0.5
-0.75
-1
-1.25
-1.5
-1.75
-2
Cp
0.0
0.025
0.05
0.075
0.9
0.925
0.95
0.975
1
X

FIGURE 8

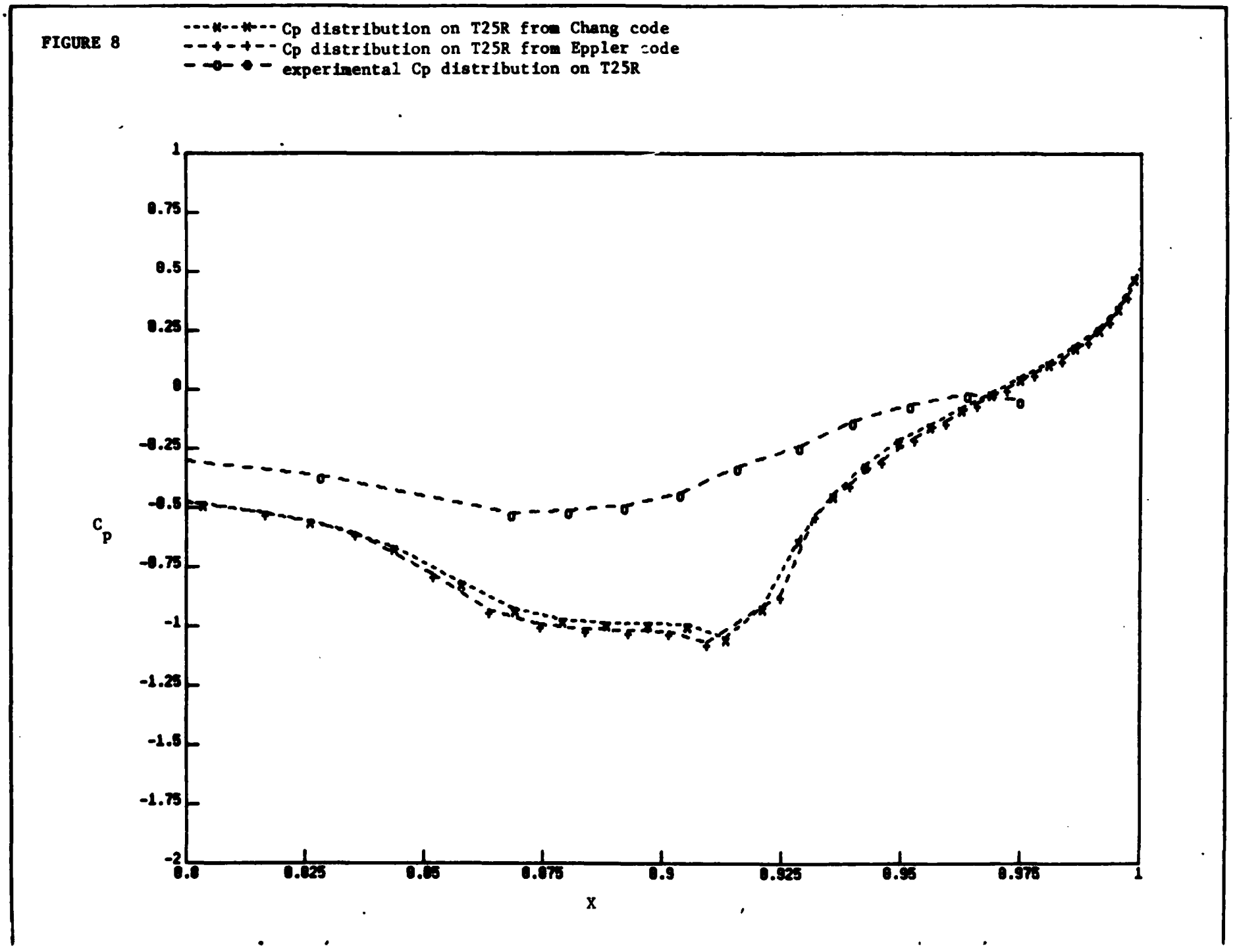
---*---*--- Cp distribution on T25R from Chang code
--+--+--- Cp distribution on T25R from Eppler code
--o--•-- experimental Cp distribution on T25R
1
0.75
0.5
0.25
0
-0.25
-0.5
-0.75
-1
-1.25
-1.5
-1.75
-2
Cp
0.0
0.825
0.85
0.875
0.9
0.925
0.95
0.975
1
X

FIGURE 9

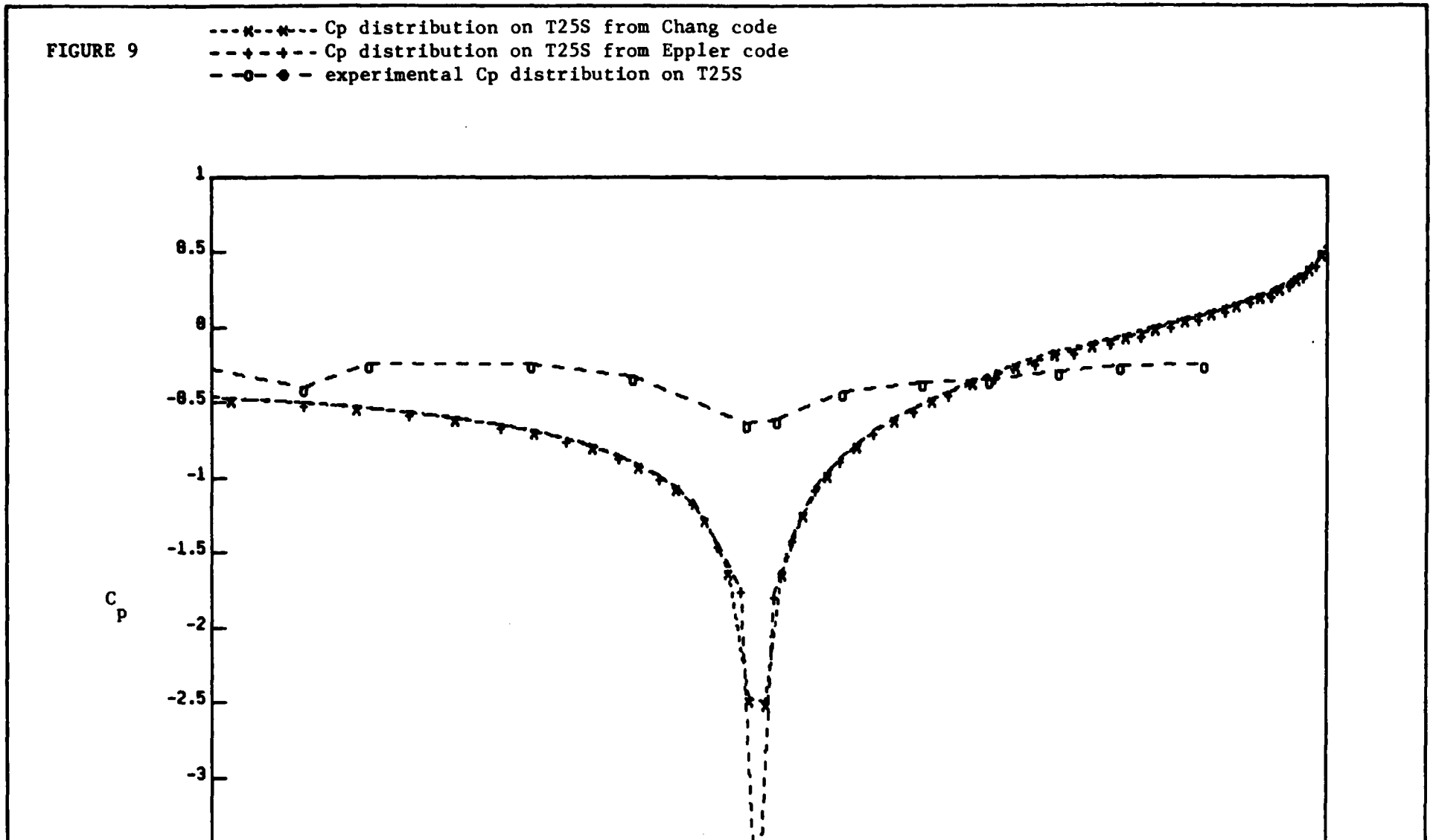
Cp distribution on T25S from Chang code
Cp distribution on T25S from Eppler code
experimental Cp distribution on T25S
1
0.5
0
-0.5
-1
-1.5
-2
-2.5
-3
-3.5
-4
-4.5
Cp
0.0
0.025
0.05
0.075
0.9
0.925
0.95
0.975
1
X

The measured pressure magnitudes on the three trailing edge sections tend to be considerably less than the predicted values, except near the trailing edge, where the predicted and measured values cross over. This same trend of lower measured Cp magnitude, relative to the predicted magnitudes, is seen for the AB5 foil in Figure 10.

The difference between the experimental and predicted Cp values can be traced, to a large extent, to the large scale trailing edge separation that occurs in each of the four airfoile being considered here (Table 7). Under conditions of strong separation the Kutta condition no longer applies at the trailing edge, thus violating one of the basic assumptions of the Eppler and Chang codes.

Another consequence of the trailing edge separation is that the separation effectively entails a large displacement thickness, which needs to be taken into consideration in the external pressure calculations. As discussed earlier, however, none of the computer codes considered here allows for any viscid-inviscid interaction.

It should be mentioned that in nonseparating flow conditions the Eppler and Chang potential flow codes have predicted pressure distributions in good agreement with experimental data.

SEPARATION

Determination of the presence and location of separation is an important factor in the design and analysis of airfoils. The eddy viscosity and k-ε codes interpret separation as being the point where the velocities become negative. Due to the singular nature of the equations (Cebeci et al, 1977) at this point, the calculations are halted. The Eppler integral code takes turbulent separation to be the point where the shape factor H_{32} becomes equal to 1.46. H_{32} is defined as δ_3/δ_2, where δ_3 is the energy thickness, given by

$$\delta_3 = \int_o^\infty \left(1-\left(\frac{u}{Uo}\right)^2\right)\frac{u}{Uo}\,dy \qquad (1)$$

and δ_2 is the momentum thickness,

$$\delta_2 = \int_o^\infty \left(1-\frac{u}{Uo}\right)\frac{u}{Uo}\,dy \qquad (2)$$

FIGURE 10

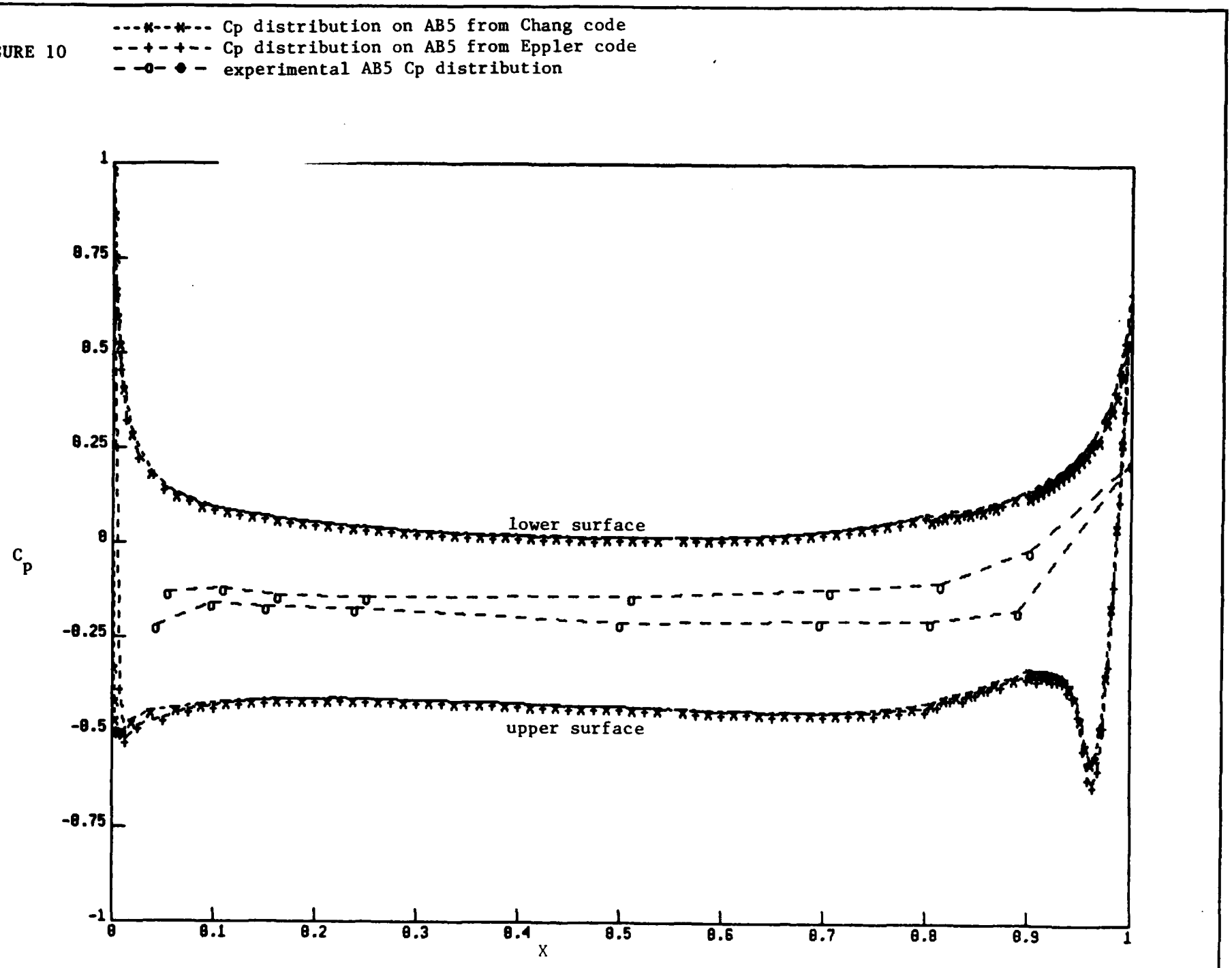
---*--*--- Cp distribution on AB5 from Chang code
--+-+-- Cp distribution on Eppler code
--o-●-- experimental AB5 Cp distribution
1
0.75
0.5
0.25
0
-0.25
-0.5
-0.75
-1
Cp
lower surface
upper surface
0
0.1
0.2
0.3
0.4
0.5
0.6
0.7
0.8
0.9
1
X

where u(x,y) is the tangential velocity component within the boundary layer. For later reference, the displacement thickness (δ_1) is defined as

$$\delta_1 = \int_0^\infty \left(1-\frac{u}{Uo}\right)dy$$

The experimentally determined Cp distributions for the airfoils were used as input in the Cebeci eddy viscosity and Cebeci κ-ϵ boundary layer codes. The codes did not predict separation for any of the airfoils; this is explained by noting that the Cebeci codes are based on thin boundary layer theory, and do not account for the large displacement effect resulting from separation.

Another contributing factor may be errors in the experimental data, resulting from the likelihood that the experiments are not exactly two dimensional.

Unlike the Cebeci codes, which require the inviscid pressure distribution as part of the program input, the Eppler code calculates the inviscid pressure distribution, and then uses it as input to the integral boundary layer analysis. Given the differences between the observed and predicted Cp distribution, it is not considered worthwhile to discuss the Eppler integral boundary layer results, as based on the predicted pressure distribution.

BOUNDARY LAYER PROPERTIES

Measured and predicted values of displacement thickness (δ_1) and momentum thickness (δ_2) for T25R are given in Tables 8 and 9. The mixing length and κ-ϵ codes are seen to give approximately the same estimates for δ_1 and δ_2. Considering that the same pressure distribution was used as input in both of these programs, this is perhaps not too surprising.

From Tables 8 and 9 it is seen that the values of δ_1 and δ_2 are slightly underpredicted, but correct within a factor of two. As explained earlier, these differences can likely be attributed to the fact that the Cebeci codes do not allow for any viscid-inviscid interaction, which will be important for strongly separated flows, such as those considered here.

Airfoil	Separation point
T45	.956
T25R	.947
T25S	.902
AB5	.962

TABLE 7 - Measured turbulent separation point (non dimensionalized by chord length) for airfoil geometries.

chord length		.78	.85	.90	.902
Experiment		.073	.045	.093	.118
Computer Code	Cebeci eddy viscosity	.065	.059	.071	.082
	Cebeci κ-ε	.065	.059	.064	.082

TABLE 8 - Measured and predicted values of displacement thickness (in.) for T25R.

chord length		.78	.85	.90	.92
Experiment		.059	.040	.050	.068
Computer Code	Cebeci eddy viscosity	.049	.045	.052	.059
	Cebeci κ-ε	.050	.046	.049	.060

TABLE 9 - Measured and predicted values of momentum thickness (in.) for T25R.

SUMMARY AND CONCLUSIONS

Four computer codes for the analysis of flow over two dimensional airfoils were exercised in comparisons against experimental data from two wind tunnel studies, involving four airfoil geometries. The shape of these airfoils (called T45, T25R, T25S, and AB5) were shown in Figures 1 and 2.

The four computer codes are designed as the Eppler potential/integral code, the Cebeci eddy viscosity code, the Cebeci κ-ϵ code, and the Chang potential code. The Eppler potential code uses vorticity distributed around a curved airfoil to obtain the inviscid flow; the integral code uses integral methods to obtain the boundary layer solution. It is the only code considered here which has both inviscid and boundary layer routines. The eddy viscosity and κ-ϵ codes solve for the vertical variation of flow quantities within the boundary layer using finite difference methods. Neither of these codes estimate the external inviscid flow field, which must be specified in the input. The Chang potential code uses a distribution of vortices and sources to determine the inviscid flow solution, and does not include any boundary layer calculations.

Numerical predictions of the codes were compared against experimental data from four airfoil geometries for pressure distribution, separation, and boundary layer properties over the airfoils. The pressure distributions over the airfoils as predicted by the Eppler and Chang potential codes agree well with each other, but are generally larger by almost a factor or two than the measured values. This is likely due to the neglect of viscid-inviscid interaction routines in the computer programs, and the likelihood that the experiments were not exactly two dimensional.

The Cebeci mixing length and κ-ϵ codes, using the experimental pressure distributions as input, did not predict the occurence of separation. The boundary layer properties for T25R were slightly underpredicted, but correct within a factor or two.

Perhaps the most important reason behind the differences in observed and predicted flow parameters is the occurance of relatively large scale separation (about 5%) in the airfoils considered here. Under these conditions, an iterative approach should be used which takes into account the effect of fluid viscosity on the external pressure field. Again, however, under nonseparating flow conditions, the programs considered here have been shown to give good agreement with experimental data in many situations.

REFERENCES

1) Chang, M.S., and Y.T. Shen (1982). Computer Programs, "Hydrofoil and Airfoil" for Calculation of Potential Flow About Two Dimensional Foils. DTNSRCC/SPD-1037-01.

2) Eppler, R., and D.M. Somers. A Computer Program for the Design and Analysis of Low Speed Airfoils. NASA Technical Memorandum 80210.

3) Cebeci, T. (1978). A Computer Program for Calculating Incompressible and Turbulent Boundary Layers on Plane and Axisymmetric Bodies With Surface Roughness. Office of Naval Research, Contract No. N00014-77-C-0156, Report No. TR-78-1.

4) Cebeci, T., and P. Bradshaw (1977). Momentum Transfer in Boundary Layers. Chapter 6. Hemisphere Publishing Corporation, Washington.

5) Blake, W.K. (1975). A Statistical Description of Pressure and Velocity Fields at the Trailing Edges of a Flat Strut. DTNSRDC Report 4241.

6) Bradshaw, P., T. Cebeci, and J.H. Whitelaw (1981). Engineering Calculation Methods for Turbulent Flow. Academic Press, New York.

DTNSRDC ISSUES THREE TYPES OF REPORTS

1. DTNSRDC REPORTS, A FORMAL SERIES, CONTAIN INFORMATION OF PERMANENT TECHNICAL VALUE. THEY CARRY A CONSECUTIVE NUMERICAL IDENTIFICATION REGARDLESS OF THEIR CLASSIFICATION OR THE ORIGINATING DEPARTMENT.

2. DEPARTMENTAL REPORTS, A SEMIFORMAL SERIES, CONTAIN INFORMATION OF A PRELIMINARY, TEMPORARY, OR PROPRIETARY NATURE OR OF LIMITED INTEREST OR SIGNIFICANCE. THEY CARRY A DEPARTMENTAL ALPHANUMERICAL IDENTIFICATION.

3. TECHNICAL MEMORANDA, AN INFORMAL SERIES, CONTAIN TECHNICAL DOCUMENTATION OF LIMITED USE AND INTEREST. THEY ARE PRIMARILY WORKING PAPERS INTENDED FOR INTERNAL USE. THEY CARRY AN IDENTIFYING NUMBER WHICH INDICATES THEIR TYPE AND THE NUMERICAL CODE OF THE ORIGINATING DEPARTMENT. ANY DISTRIBUTION OUTSIDE DTNSRDC MUST BE APPROVED BY THE HEAD OF THE ORIGINATING DEPARTMENT ON A CASE-BY-CASE BASIS.

END

FILMED

9-85

DTIC